JOURNAL OF MATERIALS SCIENCE 22 (1987) 3974–3982

Segregation at the {0 1 3} symmetrical tilt grain boundary in dilute Fe–Si alloy bicrystals

P. LEJČEK, J. BRÁDLER, V. PAIDAR
Institute of Physics, Czechoslovak Academy of Sciences, Na Slovance 2, 180 40 Prague 8, Czechoslovakia

M. KOUTNÍK
National Research Institute for Materials, Opletalova 25, 113 12 Prague 1, Czechoslovakia

The structure and segregation behaviour of the {0 1 3} symmetrical tilt grain boundary were studied in Fe–Si dilute alloy bicrystals. Structural features such as twins, cleavage tongues and steps at the grain boundary, revealed by brittle intercrystalline fracture, are described and the identity of the fracture surface with the grain boundary is discussed. The amounts of segregation of phosphorus and silicon obtained by Auger electron spectroscopy are correlated with the structure of the analysed regions. The scatter of measured values of concentration of phosphorus and silicon in different regions of the fracture surface is explained from a structural point of view. A repulsive interaction between phosphorus and silicon atoms was confirmed. Grain-boundary enrichment ratios for phosphorus of 185 and 278, and decreases of the silicon concentration to 63 and 60% of the bulk value, were found at the grain boundary in as-grown and annealed bicrystals, respectively.

1. Introduction

Many studies of grain-boundary segregation have been performed to explain various effects dependent on the chemical composition in the vicinity of the boundary. Auger electron spectroscopy (AES) of grain boundaries revealed by means of intergranular fracture is mainly employed for these investigations [1]. Polycrystalline samples have mostly been studied [2–6]. On the basis of the results obtained several authors have suggested that orientation dependence of grain-boundary segregation is responsible for the spread of the measured values of chemical composition [1, 7–10]. This suggestion was confirmed by measurements on individual facets in polycrystals by Briant [10]. Nevertheless, the study of the anisotropy of solute segregation to a single well-defined grain boundary in bicrystals has been reported in only a few papers [11–14]. In these papers only limited attention was paid to a detailed observation of the fracture surface and to verification of its identity with the grain boundary. Such observations seem to be very important for determination of the level of solute segregation to well-defined grain boundaries. There are local inhomogeneities on the fracture surface which originated during the fracture process and which can remain unrevealed by the scanning electron microscopy (SEM) image of commonly used AES apparatuses. These inhomogeneities can affect the measured values of chemical composition of the fracture surface. Moreover, the observations of grain boundaries revealed by intercrystalline fracture seem to be very useful for the investigation of the internal structure of grain boundaries over submicrometre areas.

The aim of present work is a detailed study of the nearly {0 1 3} symmetrical tilt grain boundary in Fe–6.14 at % Si alloy bicrystals, revealed by means of brittle intercrystalline fracture. The types of structural feature characteristic of this boundary are outlined. AES measurements of phosphorus as a major impurity and of silicon at the fracture surface are presented, and the correlation of the values obtained with the grain-boundary structure is discussed.

2. Experimental methods

The bicrystals of Fe–Si dilute alloy of composition given in Table I were grown by means of a floating zone technique with two single-crystalline parts in the desired crystallographic orientation used for seeding. As-grown bicrystals had a cylindrical shape of 13 mm diameter and up to 60 mm length, with a macroscopically planar boundary parallel to the growth axis [15]. The normal to the boundary plane deviated about 3° from the ⟨0 1 3⟩ crystallographic direction in the bicrystal used for our study. Samples with a diameter of 3.7 mm having the boundary plane perpendicular to their axes were cut from as-grown bicrystals. For comparison, some samples were annealed for 120 h at 1023 K in a hydrogen atmosphere and slowly cooled ($120\,K\,h^{-1}$). All the samples were notched at the boundary to a diameter of about 1.5 mm and adapted by means of brass extensions to the dimensions of standard AES specimens (total length of 35 mm).

All samples were broken by impact bending in the ultra-high vacuum chamber of the AES apparatus (PHI 545 A, Physical Electronics Industry) at a temperature of about 210 K and a vacuum of about

0022–2461/87 $03.00 + .12

TABLE I Chemical composition of Fe–Si alloy bicrystals

Element	Si	Ni	Cu	Mn	P	C	N	O	S	Fe
Content (at %)	6.14	0.14	0.009	0.015	0.026	0.0086	0.0077	0.0034	0.001	Balance

4×10^{-8} Pa. The revealed fracture surface was inspected in the SEM mode and analysed by means of Auger electrons for at least 10 points on the fracture surface. The experimental conditions for AES were as follows: primary beam energy 5 keV and diameter 3 μm, modulation 6 eV, time constant 1 msec, sweep rate 1.5 eV sec^{-1}. Depth profiling was performed using argon ion bombardment with an energy of 3 keV at a heating current of 25 mA and an argon pressure of about 7×10^{-3} Pa.

After removal from the AES apparatus, both halves of each fractured sample were studied by the following additional methods: optical microscopy with Nomarski interference contrast (Opton Photomicroscope), SEM (Jeol 733 Superprobe) and X-ray back-reflection topography (Co$K\alpha$ radiation, 0 0 2 and $\bar{1}$ 1 2 reflections).

3. Results of AES measurements

The fracture surface of each sample was analysed by means of AES at several points. Phosphorus and silicon were detected as the main impurity and alloying element, respectively. A characteristic spectrum of Auger electrons is shown in Fig. 1a. Typical values obtained from the fracture surfaces of both as-grown and annealed bicrystals are presented in Tables II and III. These give the measured values of silicon and phosphorus relative peak height (r_{Si} at 92 eV and r_P at 120 eV, respectively) with respect to the iron peak (at 47 eV), their average values, A, and standard deviations, σ.

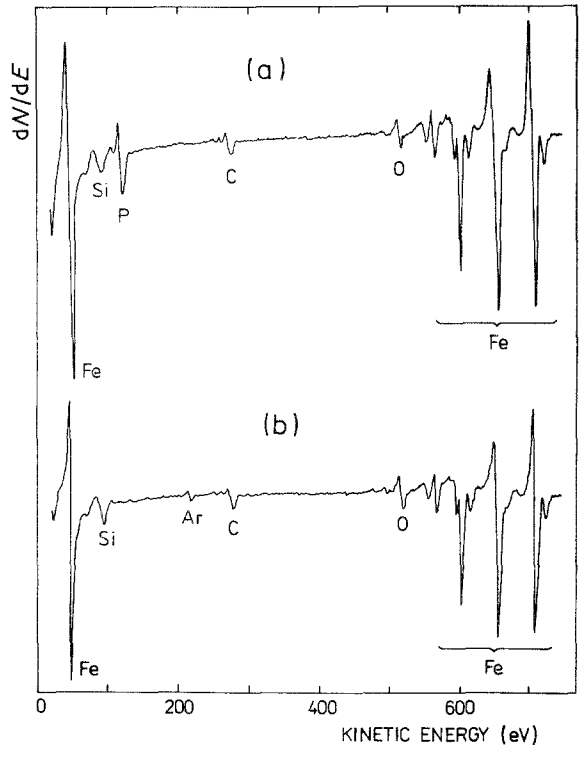

Figure 1 Auger electron spectra taken from the same point of the grain-boundary fracture surface of annealed bicrystal (a) before and (b) after 6 min argon ion sputtering.

After recording all AES data from the fracture surface, depth profiling at a chosen point was done by argon ion sputtering. Under the conditions mentioned a layer of approximately 2 nm thickness was removed during 1 min of sputtering. The changes of the phosphorus and silicon peak heights during this process are shown for both kinds of sample in Fig. 2. After profiling no phosphorus was detected by AES (Fig. 1b). The values of r_{Si} after deep sputtering (more than 5 min) were practically the same for the annealed (0.10) and for the as-grown (0.11) bicrystals.

Small peaks of nitrogen were observed in the spectra taken from the grain boundary of the as-grown bicrystal only. During sputtering its height rapidly decreased to below the detection limit. Peaks for carbon and oxygen were found in all spectra. Their height also decreased during sputtering; however, as soon as the bombardment was stopped, these elements appeared again on the analysed surface. To estimate the level of grain-boundary segregation we used the standard procedure for the evaluation of experimental data [16]. Calculated concentrations of phosphorus, silicon and nitrogen and corresponding grain-boundary enrichment ratios for as-grown and annealed bicrystals are given in Table IV. No correction to the depth distribution of segregating elements has been done.

4. Observations of grain-boundary fracture surface

A typical example of the grain-boundary surface revealed by intercrystalline fracture, imaged by means of different techniques, is shown in Fig. 3. The first impression from the secondary electron image (Fig. 3a), which is the only possibility of observation of the fracture surface in the AES apparatus, is that the surface is flat with only a few linear traces. Conventional optical microscopy does not give any better information (Fig. 3b). However, the use of Nomarski interference contrast enables us to distinguish more details on the surface. A long-period surface waviness is clearly seen, and less pronounced inhomogeneities are also visible (Fig. 3c). The observations were completed by X-ray topography (Fig. 3d) and more thorough investigations of the fracture surface were performed by means of the above-mentioned microscopical techniques at higher magnifications.

The following structural features were found on the fracture surfaces of both as-grown and annealed bicrystals:

(a) Regions of transgranular cleavage. Transgranular cleavage may occur during fracture, usually only at peripheral regions of the fracture surface where the fracture process either began or terminated (see Fig. 3). Typical patterns of transgranular cleavage are visible there. The presence of such regions is usually

TABLE II AES analyses of grain-boundary fracture surface of as-grown bicrystals: r_{Si} and r_P are relative peak heights of silicon and phosphorus, respectively, A is the average value and σ is the standard deviation

Relative peak height	Point No.										A	σ	σ/A (%)
	1	2	3	4	5	6	7	8	9	6*			
r_{Si}	0.126	0.108	0.100	0.098	0.102	0.093	0.096	0.092	0.086	0.094	0.096	0.0117	12
r_P	0.139	0.130	0.124	0.115	0.125	0.137	0.148	0.139	0.175	0.138	0.137	0.0164	12

*Repeated measurement after analyses at all other points.

TABLE III AES analyses of grain-boundary fracture surface of annealed bicrystal

Relative peak height	Point No.												A	σ	σ/A (%)
	1	2	3	4	4*	5	6	7	8	9	10	5†			
r_{Si}	0.110	0.098	0.102	0.103	0.097	0.075	0.075	0.071	0.069	0.065	0.067	0.069	0.083	0.0171	21
r_P	0.093	0.123	0.147	0.111	0.112	0.202	0.197	0.195	0.186	0.159	0.188	0.217	0.161	0.0424	26

*Repeated measurement.
†Repeated measurement after analyses at all other points.

already apparent from the secondary electron image of the AES apparatus.

(b) Twins. Twinning occurs in the vicinity of the grain boundary during low-temperature deformation leading to fracture. As for transcrystalline cleavage, intensive twinning appears mostly in regions of initial and terminating fracture at the periphery of the fracture surface. The twins are relatively very large in these regions and their main trunks have many branches (Fig. 4). The twinning occurs in several systems. Since we observe the intersections of twins with only one surface, we are not able to determine these systems unambiguously. From crystallographic analysis we suppose that twinning occurs in the following four systems: $(1\,\bar{1}\,2)[\bar{1}\,1\,1]$, $(1\,1\,2)[\bar{1}\,\bar{1}\,1]$, $(\bar{1}\,\bar{1}\,2)[1\,1\,1]$ and $(\bar{1}\,1\,2)[1\,\bar{1}\,1]$ in the coordinate system where the boundary normal is $[0\,1\,3]$ and the impact direction is approximately $[\bar{3}\,3\,\bar{1}]$.

(c) Cleavage tongues. These represent another kind of inhomogeneity appearing on the grain-boundary

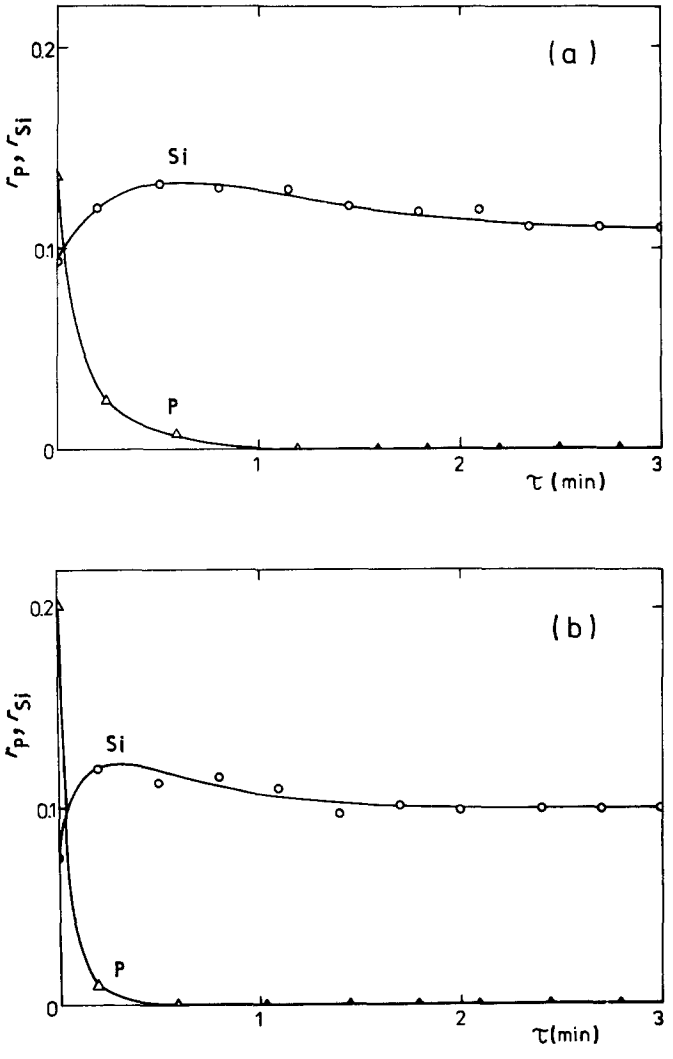

Figure 2 Variation of silicon and phosphorus concentrations (represented by r_P and r_{Si}) with time τ of sputtering on nearly $\{0\,1\,3\}$ symmetrical tilt boundary of (a) as-grown and (b) annealed bicrystals.

TABLE IV Grain-boundary concentrations, C_i^{GB}, of phosphorus, silicon and nitrogen, and corresponding grain-boundary enrichment ratios, β_i', for as-grown and annealed bicrystals

Bicrystal type	C_P^{GB} (at %)	C_{Si}^{GB} (at %)	C_N^{GB} (at %)	β_P'	β_{Si}'	β_N'
As-grown	4.81	3.89	1.57	185	0.63	204
Annealed	7.23	3.71	–	278	0.60	–

surface as a consequence of the fracture process. Usually the cleavage tongues are straight steps of changing width (Fig. 5). They are of the same origin as those which occur at a brittle transcrystalline cleavage [17]. During fracture a large amount of stress is accumulated at the crack tip. When the crack tip meets any structural obstacle such as a precipitate, twin (Fig. 6) or local transgranular crack, this stress can cause a local change of the cracking plane. However, cracking along a new plane (i.e. transcrystalline cleavage) is less favourable than grain-boundary fracture. Therefore, the fracture returns back to the boundary plane and proceeds along it together with the front of the main crack. Straight cleavage tongues of various dimensions lying along the intersections of the $\{1\,1\,2\}$ planes and the boundary surface then remain on the surface. The length and the width of cleavage tongues range from 1 to 10^3 μm and from 10^{-1} to 1 μm, respectively. Because of the large amount of strain accompanying surface inhomogeneities, cleavage

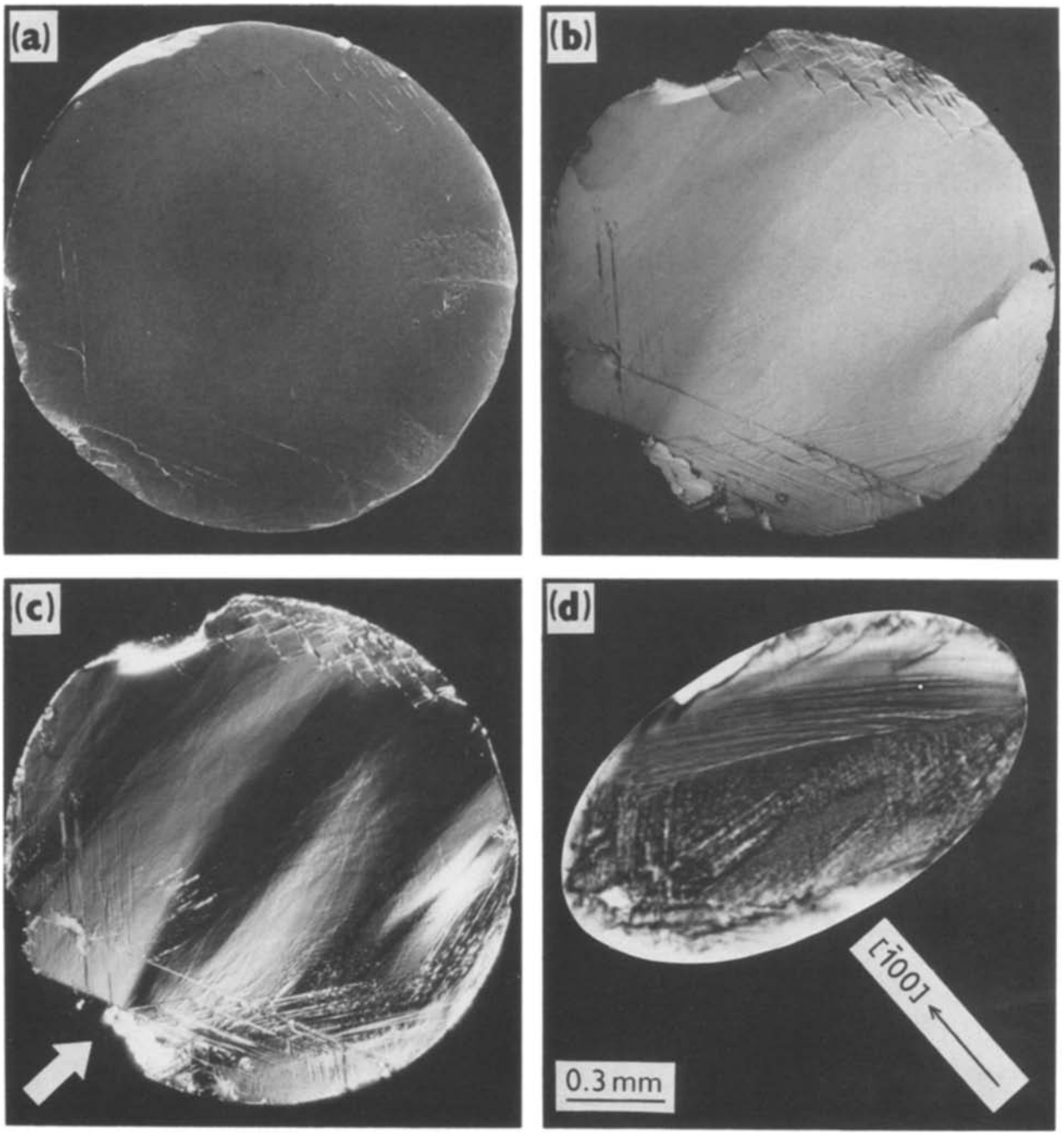

Figure 3 Fracture surface along nearly $\{0\,1\,3\}$ symmetrical tilt grain boundary in Fe–6.14 at % Si alloy bicrystal in as-grown state. (a) Secondary electron image of AES apparatus, (b) conventional optical microscopy, (c) optical microscopy with Nomarski interference contrast (the arrow indicates the impact direction) and (d) X-ray back-reflection topograph (Co$K\alpha$ radiation, 0 0 2 reflection; the arrow shows the $[\bar{1}\,0\,0]$ crystallographic direction).

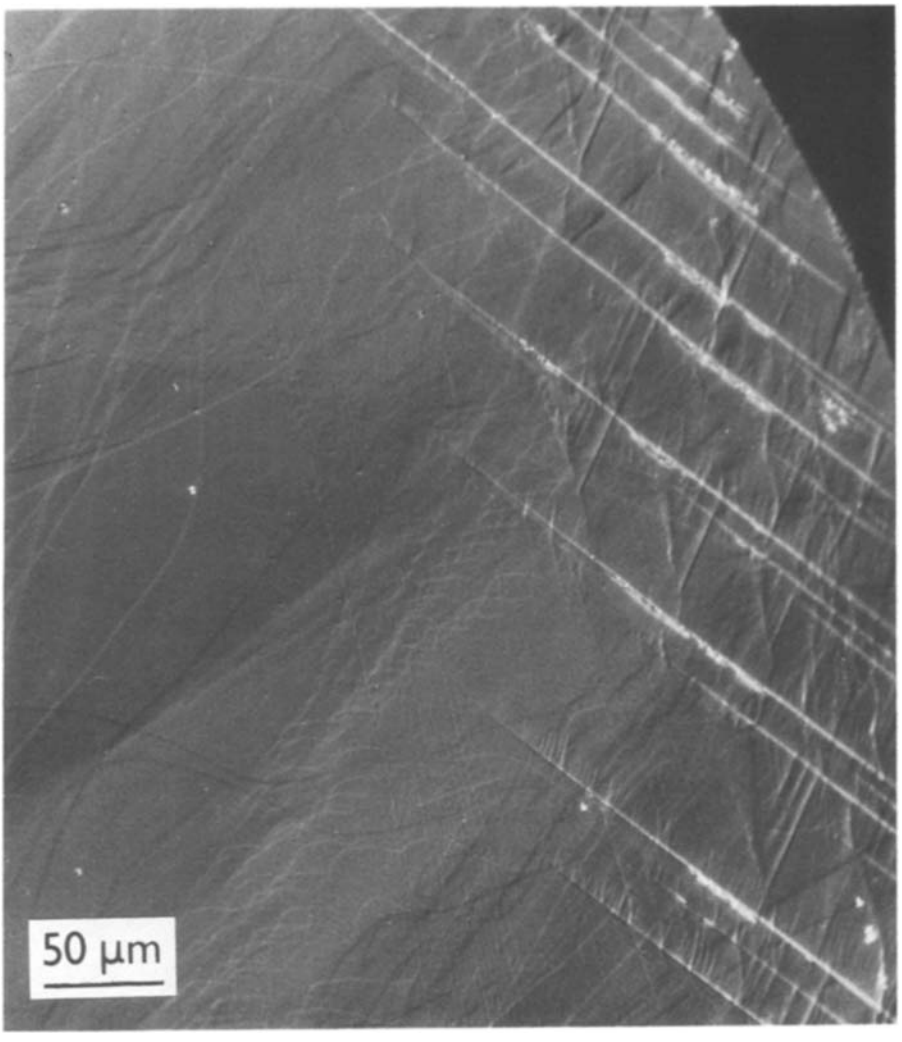

Figure 4 Peripheral region of fracture surface. Many twins are present on the right-hand side. There are several sets of steps on the left. Optical microscopy with Nomarski interference contrast.

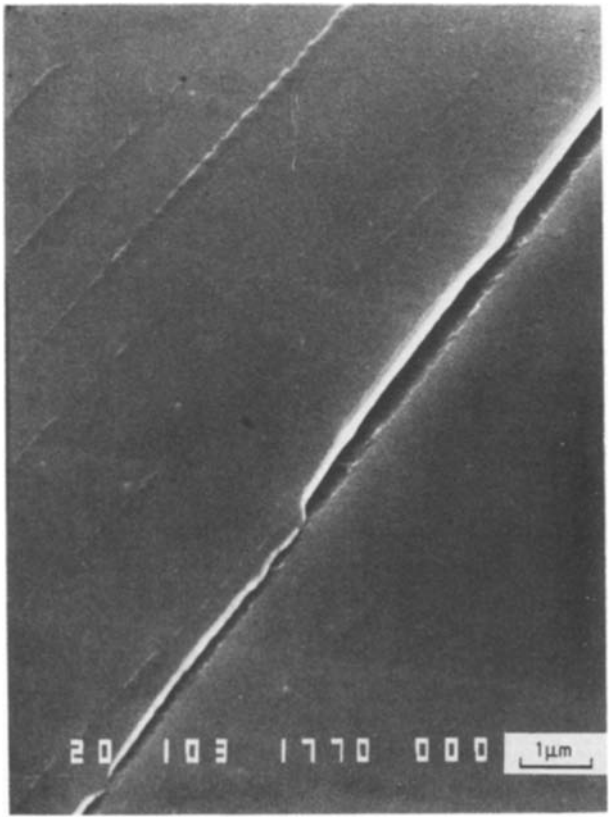

Figure 5 Cleavage tongue on grain boundary. On the left-hand side, the remnants of cleavage tongues from the other half of the specimen are apparent. Scanning electron microscopy.

tongues give rise to a pronounced contrast in X-ray topographs (Fig. 3d) as described by Gronwald and Henzler [18].

(d) Steps on the fracture surface. Besides twin traces we observed various thin lines on the fracture surface. Some of them are straight and almost regular in their spacing, while others are curved and rather randomly distributed (see Figs 4 and 6). These lines may correspond to small surface steps. The dimensions of the regular steps in Fig. 7 (black lines) are a height and spacing of the order of 10 nm and 1 μm, respectively. The height of the irregular steps (left-hand side in Fig. 4) was estimated to be of a comparable magnitude. Since the regular fine steps are not affected by the intersecting traces with cleavage tongues in Fig. 7 we can suppose that these steps had been formed before twinning and cleavage took place in the fracture process. Two hypotheses can be put forward for the origin of the steps. The steps could be related to lattice dislocations and may represent slip lines, or they could be related to grain-boundary faceting. In the former case the steps are created during the fracture process, while in the latter case they are part of the internal grain-boundary structure because they are geometrically necessary. If the facets lie on {0 1 3} then the steps between facets compensate for the deviation of the macroscopic boundary plane from the {0 1 3} plane which may be energetically favourable. The

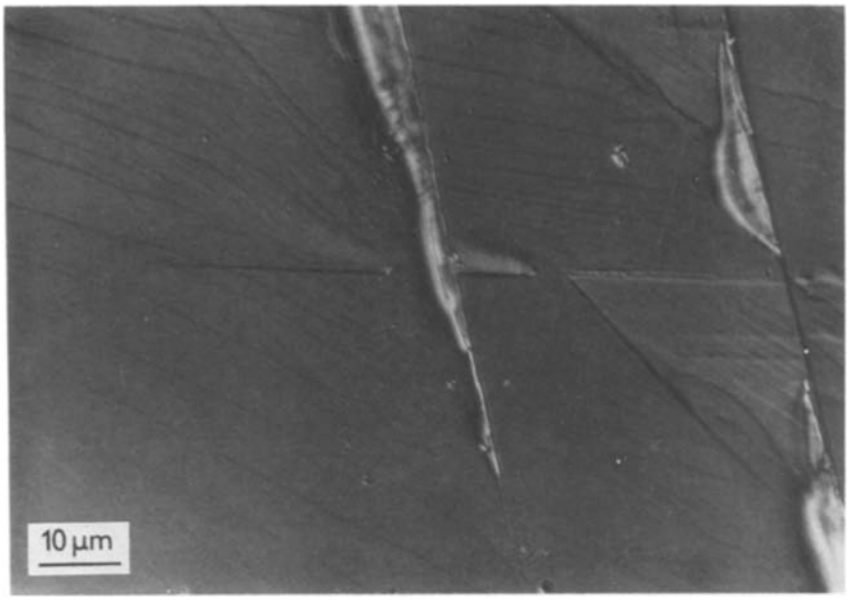

Figure 6 Cleavage tongues occurring along twins. Very fine steps are visible on the background. Optical microscopy with Nomarski interference contrast.

inclination of the boundary to the {0 1 3} plane varies locally (notice a slight boundary waviness apparent in Fig. 3c) and hence the width of facets may also vary correspondingly. Let us note that some steps terminate on subgrain boundaries (Fig. 8) but others penetrate freely from one mosaic block to another, as would be expected in the case of slip traces. It seems to us that both possibilities must be considered. In some cases (see Fig. 6) the fine steps interact with twins and are presumably connected with plastic deformation, while in other cases (Fig. 7) the steps may represent the grain-boundary structure.

5. Discussion

Based on observations of the structure of the fracture surface we can conclude that the actual grain boundary is mostly revealed during fracture under the above-mentioned experimental conditions. Except for some regions at the periphery of the fracture surface, no patterns typical of transcrystalline cleavage were detected. The shapes of cleavage tongues suggest that the boundary plane is more suitable for crack propagation than other (crystallographic) planes. Many steps on the fracture surface and their behaviour seem to be characteristic of the grain boundary. The level of segregation on the fracture surface also supports the idea of the identity of the fracture surface with the grain boundary.

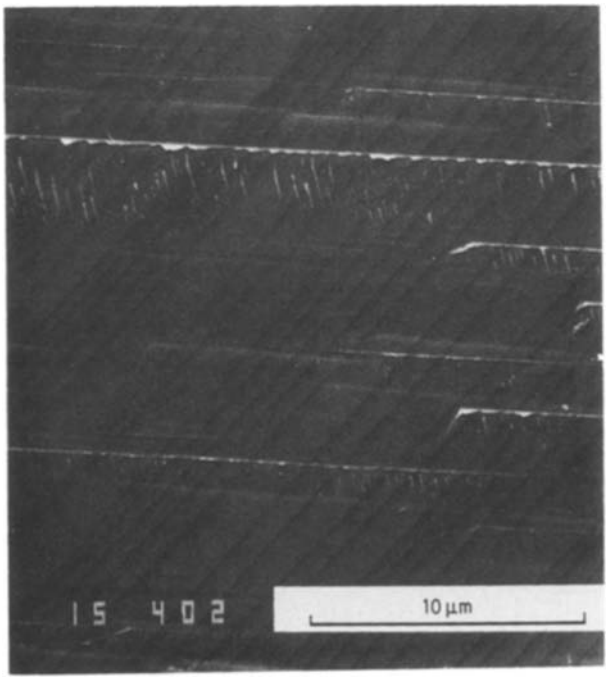

Figure 7 Set of nearly parallel almost regular steps on fracture surface (black lines) and another system of parallel traces with cleavage tongues. Scanning electron microscopy.

Rather little attention has been paid to the structure of surfaces revealed by brittle intergranular fracture in previous papers on segregation effects. The structures of fracture surfaces of well-defined grain boundaries were presented in a few cases, e.g. in Fe–Si and Fe–Sn alloys [11], in Cu–Sb alloy [13] or in molybdenum [19, 20], but no details have been discussed. Marayuma *et al.* [21] presented magnified views of grain-boundary facets in polycrystalline iron. Twins, cleavage tongues and also inclusions are seen in their micrographs (Figs 9 and 10 in [21]) but no boundary steps are visible there. In other papers on polycrystals, the authors acquiesce in stating the identity of grain boundaries with individual facets of the fracture surface without any detailed observation of their structure (e.g. [2, 10]). It seems that the only evidence for this identity (even though it is very substantial) results from the presence of segregating elements on the fracture surface.

It is apparent in Fig. 1 that traces of carbon and oxygen are present in the spectra taken from the as-fractured surface as well as from the sputtered one. Their contents decrease rapidly to below the detection limit during sputtering, but they appear again immediately after the ion bombardment is stopped. It seems that their occurrence is not only a segregation effect but rather a consequence of rapid contamination of the surface from the residual atmosphere in the AES apparatus. Their presence will not be further considered.

The concentration depth profiles of phosphorus and silicon are shown in Fig. 2. The phosphorus concentration reaches a maximum value at the boundary

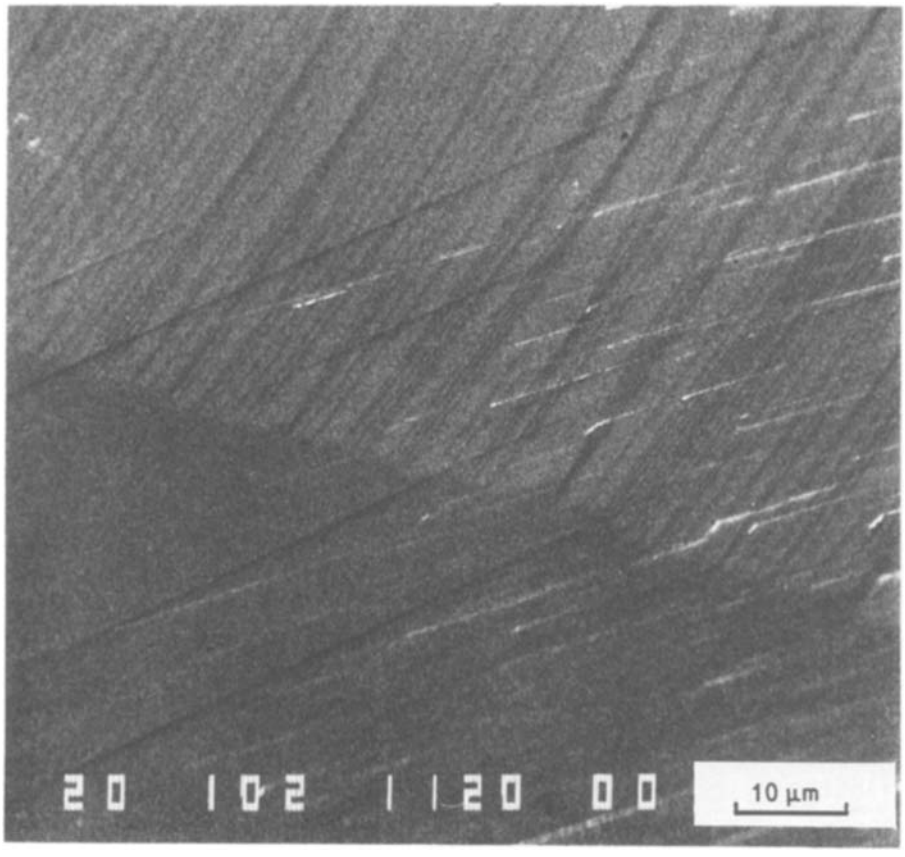

Figure 8 The intersection of a mosaic block boundary with the fracture surface. One set of steps terminates at this boundary, the other continues across it. Scanning electron microscopy.

and decreases below the detection limit in a distance of less than 2 nm from the boundary. The concentration of silicon is slightly lower at the boundary than in the bulk. In the vicinity of the boundary the silicon concentration increases to a maximum and then falls to the value of the bulk composition. Such shapes of concentration depth profiles suggest a repulsive interaction of phosphorus and silicon atoms in iron, as described by McMahon [22]. The same kind of P–Si interaction has been deduced from the temperature dependence of surface segregation in Fe–Si single crystals [23].

As seen from Tables II and III, the values of the relative peak heights of phosphorus (120 eV), r_P, and silicon (92 eV), r_{Si}, related to iron (47 eV) measured in different regions of the bicrystal fracture surface show a relatively large scatter. However, a graphical plot of r_P against r_{Si} (Fig. 9) shows that these values are not independent. The concentration of phosphorus systematically decreases with increasing concentration of silicon.

It is apparent from Fig. 10 that the measured values of the relative peak heights of both elements depend on the structure of the analysed regions. Regions of a chosen fracture surface where the most diverse structural features were observed are shown in Fig. 10a, which does not represent the sample depicted in Fig. 3. At regions corresponding to the boundary plane the concentration of phosphorus (represented by r_P) is relatively high (e.g. Point No. 5 in Table III and Fig. 10). On the other hand, the values of r_P taken from regions with structural imperfections induced by the fracture process (e.g. cleavage tongues and twins) are lower. In these cases, the analysed region does not lie entirely on the boundary plane. This explanation is in good agreement with the concentration profiles of phosphorus and silicon in a direction perpendicular to the boundary plane. The concentration of phosphorus decreases and that of silicon increases in layers adjacent to the boundary (Fig. 2). Thus the scatter of the measured values of r_P and r_{Si} is not caused by inaccuracy of the AES technique, but the differences

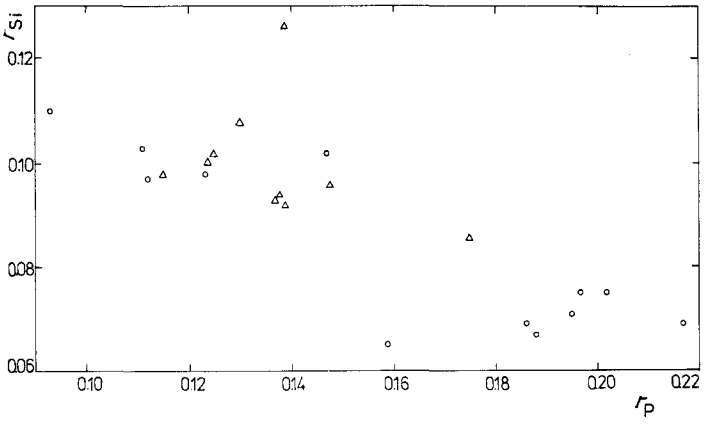

Figure 9 The mutual plot of measured values of relative peak ratios of phosphorus and silicon. (△) As-grown bicrystal, (○) annealed bicrystal.

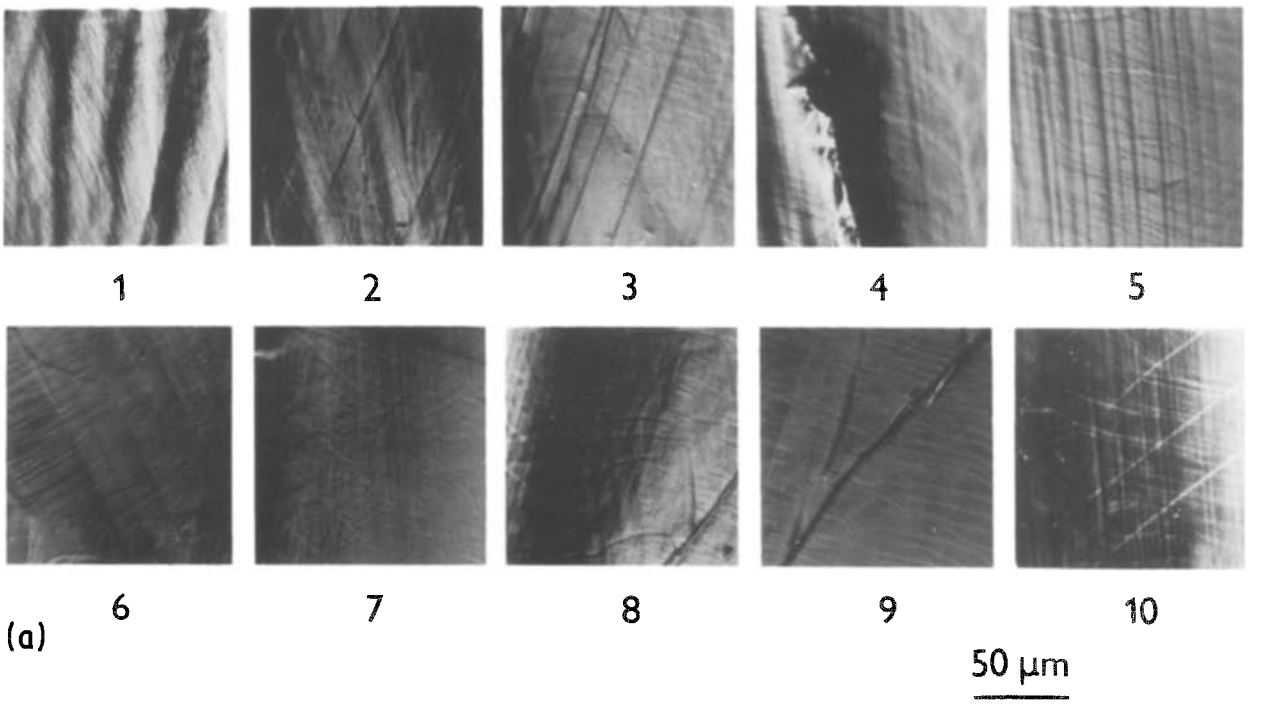

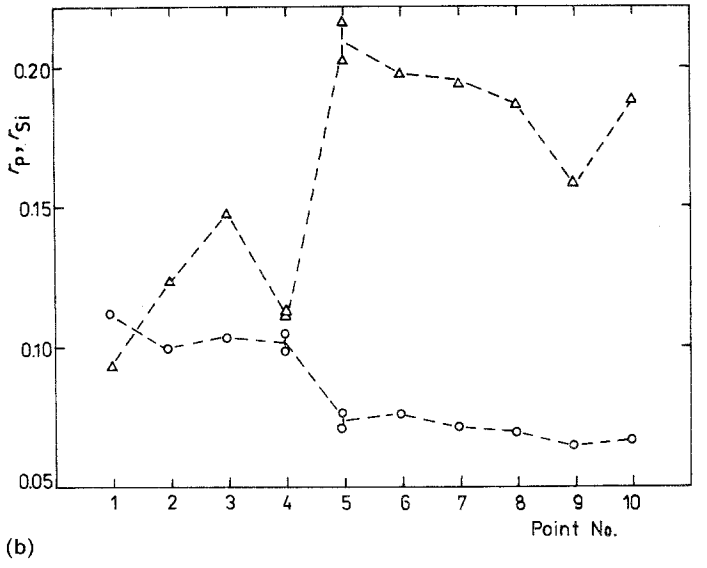

Figure 10 (a) The structure of analysed regions (optical microscopy with Nomarski interference contrast) and (b) values of (△) r_P and (○) r_{Si} taken from an area of 3 μm diameter lying in the centre of the respective regions. The dashed lines have no physical meaning.

obtained correspond to different structures of the analysed regions.

The standard deviations from the average values of r_P and r_{Si} in Tables II and III are ±12% for both phosphorus and silicon in as-grown bicrystals, and ±26% for phosphorus and ±21% for silicon in annealed bicrystals, respectively. These deviations are higher than the deviation of ±3 to 12% for antimony and phosphorus grain-boundary segregation in Ni–Cr steels when measured on a single facet of polycrystalline material by Briant [10]. The main difference between single facets in our study and his consists in their dimensions. The boundary area in our bicrystalline specimens is about 1.75 mm^2, the analysed regions are relatively distant, and the structural features of the fracture surface are diverse as discussed above, whereas the single boundary area in Briant's study [10] was at most 0.01 mm^2 and the analysed regions were close to each other. We do not know details of the fracture surface structure of Briant's individual facets, but it can be assumed that it was much more homogeneous than in our case and hence the scatter of the measured values of grain-boundary segregation is lower.

The scatter of data for the annealed bicrystal is larger than for the as-grown bicrystal due to the more pronounced segregation in annealed samples manifested in Fig. 2. The concentrations of segregated elements then change more intensively with distance from the boundary, and thus the measured values of r_P and r_{Si} are more scattered at the same level of damage of the boundary surface in the fracture process.

It follows from the above discussion that those regions with the highest values of r_P should correspond to phosphorus enrichment at the grain boundary. Because correction to the escape depth was not done, the values presented in Table IV do not represent the concentration of the boundary monolayer, but instead that of n atomic layers for each element ($n = 0.41E_{kin}^{1/2}$, where E_{kin} is the kinetic energy of Auger electrons). Thus the concentrations and also the enrichment ratios of phosphorus and nitrogen in the boundary monolayer will be higher than the given values. On the other hand, the content of silicon at the boundary might be lower. Let us note that the equilibrium state was not reached in both methods of heat

treatment used in this study. From this point of view it seems that the boundary enrichment of phosphorus is probably greater in Fe–Si alloys than that in pure iron, where it reaches values of 200 to 300 [1]. This behaviour could be rationalized in terms of solubility. Silicon decreases the solubility of phosphorus in α-Fe [24] and thus raises its segregation tendency as described by Seah and Hondros [7].

Nitrogen was detected at the grain boundaries of as-grown bicrystals only. Its absence at the boundaries of annealed bicrystals could probably be caused by the lowering of its bulk content during prolonged heating of the sample.

6. Conclusions

In the present work, structural observations of the nearly {0 1 3} symmetrical tilt grain boundary in Fe–Si dilute alloy bicrystals revealed by brittle fracture are reported. It was found that there are some structural features of the fracture surface, in particular twins and cleavage tongues, which appear as a result of the fracture process. However, there are also sets of small steps which seem to be a part of the grain-boundary structure. No qualitative differences in the grain-boundary structure were found between as-grown bicrystals and bicrystals annealed for 120 h at 1023 K in hydrogen.

The phosphorus and silicon compositions at the boundary obtained by AES were compared with the local structure of the analysed regions. It was shown that fracture surface imperfections strongly influence the level of the measured concentrations of both elements.

An enrichment of the grain boundary by phosphorus and a depletion of silicon were detected. The depth distributions of both elements demonstrate the repulsive interaction between phosphorus and silicon atoms. The repulsive interaction is also confirmed by the mutual dependence of the phosphorus and silicon concentrations at various analysed points on the fracture surface. The phosphorus and silicon concentrations are roughly inversely proportional each to the other.

The enrichment ratios of phosphorus at the grain boundary were found to be 185 and 278 for as-grown bicrystals and annealed ones, respectively. For silicon, decreases to 63 and 60% of the bulk concentration were found at the respective boundaries.

Acknowledgement

The authors are grateful to Dr S. Kadečková for the preparation of the bicrystals used in the present study.

References

1. E. D. HONDROS and M. P. SEAH, *Int. Met. Rev.* **222** (1977) 262.
2. C. J. McMAHON Jr and L. MARCHUT, *J. Vac. Sci. Technol.* **15** (1978) 450.
3. H. HÄNNINEN and E. MINNI, *Metall. Trans.* **13A** (1982) 2281.
4. C. L. WHITE, L. HEATHERLY and R. A. PADGETT, *Acta Metall.* **31** (1983) 111.
5. H. HOFMANN and S. HOFMANN, *Scripta Metall.* **18** (1984) 77.
6. W. T. NACHTRAB and Y. T. CHOU, *J. Mater. Sci.* **19** (1984) 2136.
7. M. P. SEAH and E. D. HONDROS, *Proc. R. Soc.* **A335** (1973) 191.
8. B. D. POWELL and D. P. WOODRUFF, *Phil. Mag.* **34** (1976) 169.
9. T. OGURA, C. J. McMAHON Jr, H. C. FENG and V. VITEK, *Acta Metall.* **26** (1978) 1317.
10. C. L. BRIANT, *ibid.* **31** (1983) 257.
11. T. WATANABE, S. KITAMURA and S. KARASHIMA, *ibid.* **28** (1980) 455.
12. M. BISCONDI, *J. Physique* **43** (1982) C6-293.
13. T. H. CHUANG, W. GUST, L. A. HELDT, M. B. HINTZ, S. HOFMANN, R. LUČIČ and B. PREDEL, *Scripta Metall.* **16** (1982) 1437.
14. E. SMITI, P. JOUFFREY and A. KOBYLANSKI, *ibid.* **18** (1984) 673.
15. S. KADEČKOVÁ, P. TOULA and J. ADÁMEK, *J. Crystal Growth* (1987) in press.
16. L. DAVIES, N. MacDONALD, P. PALMBERG, G. RIACH and R. WEBER, "Handbook of AES" (Physical Electronics Industry, Eden Prairie, Minnesota, 1976).
17. V. KAREL, *Z. Metallkde* **60** (1969) 298.
18. K. D. GRONWALD and M. HENZLER, *Appl. Phys.* **A34** (1984) 253.
19. H. KURISHITA, S. KUBA, H. KUBO and H. YOSHINAGA, *Trans. Jpn Inst. Met.* **26** (1985) 332.
20. V. G. SURSAEVA, V. G. GLEBOVSKY, Yu. M. SCHULGA and L. S. SCHVINDLERMAN, *Scripta Metall.* **19** (1985) 411.
21. K. MARUYAMA, M. MESHI and H. OIKAWA, *Acta Metall.* **34** (1986) 107.
22. C. J. McMAHON Jr, *Mater. Sci. Eng.* **42** (1980) 215.
23. P. LEJČEK, R. SEIDL and V. PAIDAR, *Scripta Metall.* **21** (1987) 273.
24. R. VOGEL and B. GIESSEN, *Arch. Eisenhüttenw.* **30** (1959) 619.

Received 30 October 1986
and accepted 28 January 1987